Journal of Nanobiotechnology

RESEARCH Open Access

Apoptotic vesicles (apoVs) derived from fibroblast-converted hepatocyte-like cells effectively ameliorate liver fibrosis

Zhi Zhong[1,3†], Xiu-Liang Cui[1,2†], Kun-Jiang Tan[1,2†], Xiang-Yu Wu[1], Xiang-Jie Zhu[1,4], Jiu-Yu Zhang[1,4], Wei-Jia Zhang[1], Hong-Yang Wang[1,2*†] and Pei-Lin Zhang[1,2*†]

Abstract

Liver fibrosis is a serious global health issue for which effective treatment remains elusive. Chemical-induced hepatocyte-like cells (ciHeps) have emerged as an appealing source for cell transplantation therapy, although they present several challenges such as the risk of lung thromboembolism or hemorrhage. Apoptotic vesicles (apoVs), small membrane vesicles generated during the apoptosis process, have gained attention for their role in regulating various physiological and pathological processes. In this study, we generated ciHep-derived apoVs (ciHep-apoVs) and investigated their therapeutic potential in alleviating liver fibrosis. Our findings revealed that ciHep-apoVs induced the transformation of macrophages into an anti-inflammatory phenotype, effectively suppressed the activity of activated hepatic stellate cells (aHSCs), and enhanced the survival of hepatocytes. When intravenously administered to mice with liver fibrosis, ciHep-apoVs were primarily engulfed by macrophages and myofibroblasts, leading to a reduction in liver inflammation and fibrosis. Proteomic and miRNA analyses showed that ciHep-apoVs were enriched in various functional molecules that modulate crucial cellular processes, including metabolism, signaling transduction, and ECM-receptor interactions. ciHep-apoVs effectively suppressed aHSCs activity through the synergistic inhibition of glycolysis, the PI3K/AKT/mTOR pathway, and epithelial-to-mesenchymal transition (EMT) cascades. These findings highlight the potential of ciHep-apoVs as multifunctional nanotherapeutics for liver fibrosis and provide insights into the treatment of other liver diseases and fibrosis in other organs.

Background

Liver fibrosis poses a significant global health challenge, potentially leading to liver cirrhosis and hepatocellular carcinoma, collectively referred to as end-stage liver disease [1]. With 840 million individuals suffering from chronic liver disease worldwide and 2 million annual deaths attributed to it, liver fibrosis has become a substantial healthcare burden [2].

Currently, no approved therapeutic agents are available for treating liver fibrosis or cirrhosis, and liver transplantation is hindered by organ donor shortages. Cell therapy offers a promising alternative, and various cell sources have shown efficacy in clinical practice [3–5]. However,

†Zhi Zhong, Xiu-Liang Cui and Kun-Jiang Tan contributed equally to this work.

Hong-Yang Wang and Pei-Lin Zhang jointly supervised this work.

*Correspondence:
Hong-Yang Wang
hywangk@vip.sina.com
Pei-Lin Zhang
peilinzhang8899@163.com

Full list of author information is available at the end of the article

© The Author(s) 2024. **Open Access** This article is licensed under a Creative Commons Attribution-NonCommercial-NoDerivatives 4.0 International License, which permits any non-commercial use, sharing, distribution and reproduction in any medium or format, as long as you give appropriate credit to the original author(s) and the source, provide a link to the Creative Commons licence, and indicate if you modified the licensed material. You do not have permission under this licence to share adapted material derived from this article or parts of it. The images or other third party material in this article are included in the article's Creative Commons licence, unless indicated otherwise in a credit line to the material. If material is not included in the article's Creative Commons licence and your intended use is not permitted by statutory regulation or exceeds the permitted use, you will need to obtain permission directly from the copyright holder. To view a copy of this licence, visit http://creativecommons.org/licenses/by-nc-nd/4.0/.

Graphical abstract

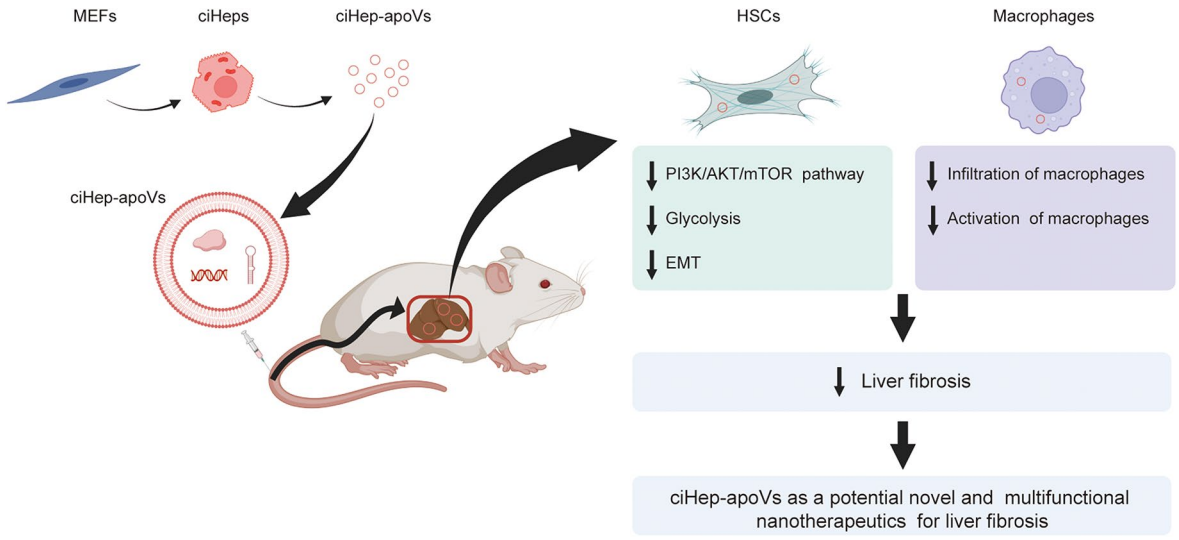

Keywords Chemical-induced hepatocyte-like cells, Apoptotic vesicles, Hepatic stellate cells, Macrophages, Multifunctional nanotherapeutics, Liver fibrosis

the quest for new cell sources to treat liver fibrosis or cirrhosis remains a pressing need. Additionally, hepatocyte transplantation is a challenging and invasive procedure, as the injection of hepatocytes through peripheral veins can lead to lung thromboembolism and animal death due to the size of hepatocytes. Therefore, portal vein injection is the most commonly used route for hepatocyte transplantation in preclinical studies. Nevertheless, this approach has drawbacks such as a high risk of bleeding, invasiveness, complexity, and potential anesthesia complications, limiting its clinical applicability.

To address these challenges, researchers have explored alternative therapies, including extracellular vesicle (EV) therapy. EVs, encompassing exosomes, microvesicles (MVs), and apoptotic vesicles (apoVs), are small membrane vesicles secreted by cells, containing biologically active molecules like proteins, nucleic acids, and lipids [6]. They play critical roles in intercellular communication and the regulation of cellular physiological and pathological states [7]. ApoVs generated during cellular apoptosis, are increasingly recognized for their significant roles in modulating immune responses and facilitating tissue renewal and regeneration [8–10]. Due to their distinct formation mechanisms, different EVs exhibit vastly disparate contents and functions. While previous studies on EVs have mainly focused on those secreted under cell survival conditions, such as exosomes [11], the understanding of apoVs remains relatively modest. However, it is becoming increasingly apparent that apoVs possess several unique therapeutic and exploitable properties compared to other types of EVs. Notably, apoVs can be easily obtained and purified [12]. Due to their encapsulation of numerous bioactive molecules and organelles, apoVs swiftly regulate intercellular signaling and have the capacity to modulate metabolic activity in recipient cells [13–15]. Phagocytes efficiently clear apoptotic cells through rapid engulfment, highlighting the crucial role of apoVs as messenger vessels among damaged cells, healthy cells, and immune cells [16]. Given the underexplored therapeutic potential of apoVs, they represent a valuable and promising area for further investigation.

In our previous investigation, we have developed a five-factor small molecule cocktail that effectively transformed mouse fibroblasts into mature, functional hepatocyte-like cells [17]. These chemical-induced hepatocyte-like cells (ciHeps) display comparable morphology, biological behavior, gene expression profiles, and functionality to primary hepatocytes. Notably, the conversion efficiency exceeds 80%, significantly surpassing other reprogramming techniques [17]. Furthermore, ciHeps have demonstrated promise for cell transplantation in liver diseases [17]. However, as outlined earlier, challenges and limitations accompany cell transplantation into the liver. Recognizing the substantial involvement of apoVs in both physiological and pathophysiological processes, along with their therapeutic and exploitable advantages, our objective is to integrate cell reprogramming technology with extracellular vesicle technology. Specifically, we aim to explore the potential therapeutic effects of liver-specific and functional

ciHeps-derived apoVs (ciHep-apoVs) in liver fibrosis, elucidating their mechanisms of action.

In this study, we generated apoVs from fibroblast-converted ciHeps by inducing cell apoptosis and found that ciHep-apoVs induced the transition of macrophages from an M1 to M2 phenotype, suppressed the activated phenotype of hepatic stellate cells (HSCs), and promoted hepatocyte viability in vitro. When administered into animals, ciHep-apoVs predominantly accumulated in the liver, alleviating inflammation and fibrosis in diseased liver in vivo. The analyses of proteomic and miRNA identified multiple functional proteins and miRNAs in ciHep-apoVs. These cargos simultaneously regulated multiple essential signaling pathways associated with fibrosis and inflammation, as well as the metabolic patterns of target cells. Collectively, our findings suggest that ciHep-apoVs hold substantial therapeutic potential for liver fibrosis, a growing global health problem.

Methods

Animal usage

This study's use of animals was approved by the Animal Care and Use Committee of the Corresponding Author's Institution. The mice were randomly assigned to different experimental groups.

Isolation and culture of mouse embryonic fibroblasts (MEFs) and mouse primary hepatocytes (MPHs)

MEFs were generated from embryos at embryonic day 13.5 (E13.5) of C57BL/6J mice. Limbs, head, tail, and internal organs were removed. The remaining tissues were cut into pieces and then trypsinized to obtain single-cell suspensions. MEFs were cultured in DMEM containing 10% FBS (Biological Industries), 100 units/ml penicillin, and 100 μg/ml streptomycin (Gibco) at 37 °C with 5% CO_2. MEFs from the 3rd to 5th generations were used in this study.

MPHs were isolated from livers of C57BL/6J mice according to a previously reported protocol [18]. The isolated MPHs were plated on rat tail collagen-coated plates for 4 h for attachment. Fresh culture medium containing DMEM plus 0.5% N2 and 1% B27 supplement (Basal Media) was used to maintain MPHs.

Isolation and culture of mouse primary hepatic stellate cells (HSCs) and peritoneal macrophages

Mouse primary HSCs were isolated from BALB/c mice (>6 month old, female, GemPharmatech Co.,Ltd, Nanjing) according to a previous study [19]. Collected HSCs were cultured in DMEM containing 10% FBS, 100 units/ml penicillin and 100 μg/ml streptomycin at 37 °C with 5% CO_2. After being cultured for 5 days, HSCs were activated to myofibroblasts (MFs).

Peritoneal macrophages were isolated from C57BL/6J mice (6 weeks, male, GemPharmatech Co.,Ltd, Nanjing), which were intraperitoneally injected with 1 ml of 3% thioglycolate broth once daily for 3 days. Then mice were sacrificed and abdominal cavity was irrigated twice with pre-cooled PBS. The cells were centrifuged, and plated in RPMI1640 plus 10% FBS, 100 units/ml penicillin and 100 μg/ml streptomycin at 37 °C with 5% CO_2 for 2 h. The non-adherent cells were removed by washing and adherent cells were peritoneal macrophages.

Immunofluorescent staining (IF)

Liver tissues were fixed with 4% paraformaldehyde (Sigma) for 24 h at 4 °C and then replaced by 30% sucrose solution for 12 h at 4 °C. A freezing microtome (Leica) was used to obtain tissue sections. Cells were fixed with 4% paraformaldehyde for 10 min at room temperature, followed by washing with PBS for 3 times. Tissue sections or cells were permeabilized with 0.3% Triton X-100 (Sigma) in PBS for 15 min at room temperature and washed with PBS for three times. After being blocked by 10% NGS(Sigma) plus 1% BSA (Sigma) in PBS for 1 h, sections or cells were incubated with primary antibodies at 4 °C overnight. Tissue sections or cells were washed three times with PBS, and then incubated with secondary antibody conjugated with fluorescence for 30 min at room temperature in dark. Hoechst 33,342 was used to stain nuclei. Antibodies used for immunofluorescent staining are listed as follows: Goat anti-Rabbit IgG (H+L) Cross-Adsorbed Secondary Antibody, Alexa Fluor™ 488 (Invitrogen, diluted 1:500), Goat anti-Rabbit IgG (H+L) Highly Cross-Adsorbed Secondary Antibody, Alexa Fluor™ 555 (Invitrogen, diluted 1:500), rabbit anti-αSMA antibody (Abcam, diluted 1:300), rabbit anti-F4/80 antibody (CST, diluted 1:200), rabbit anti-DESMIN antibody (Abcam, diluted 1:300).

Real-time fluorescent quantitative polymerase chain reaction (RT-qPCR)

Total RNA was extracted from cells or tissues with trizol (Invitrogen) protocol as recommended by manufacturer. 1 μg of RNA was used to get cDNA through reverse transcription with RevertAid First Strand cDNA Synthesis Kit (Thermo scientific) according to manufacturer's instructions. Quantitative real-time PCR was performed using SYBR Green Master Mix (Vazyme) on a Roche LightCycler480 II (Roche). Primer sequences are provided in the supplementary Table S1.

Collection and quantification of apoptotic vesicles (apoVs)

The cells were washed with PBS three times and then cultured in DMEM with EV-depleted FBS and staurosporine (STS, Target Mol). EV-depleted FBS was prepared by ultracentrifugation for 18 h at 100,000 g. After a 12-hour

treatment, the supernatant from apoptotic cells was collected and centrifuged at 800 g for 10 min. The supernatant was then filtered using a 5 μm filter and subsequently centrifuged at 16,000 g for 30 min at 4 °C. The apoVs pellet was washed twice with sterile saline solution. ApoVs were quantified by measuring protein concentration using a BCA Protein Assay Kit (Thermo Scientific). For in vitro studies, apoVs were used at a concentration of 2.5 μg/ml.

Collection and quantification of exosomes

The cells were washed with PBS three times and then cultured in DMEM with EV-depleted FBS for 48 h. After collecting the cell culture supernatant, exosomes were isolated through a series of centrifugation steps. Briefly, the supernatant was initially centrifuged at 300 g for 10 min at 4 °C, followed by centrifugation at 2000 g for 10 min at 4 °C, and then at 10,000 g for 30 min at 4 °C. Finally, the supernatant underwent ultracentrifugation at 120,000 g for 90 min at 4 °C to pellet the exosomes. The pellet was washed twice with PBS and resuspended in PBS. Exosomes were quantified by measuring protein concentration using a BCA Protein Assay Kit (Thermo Scientific). For in vitro studies, exosomes were used at a concentration of 2.5 μg/ml.

Transmission electron microscopy (TEM) observation of apoVs or exosomes

Initially, apoVs or exosomes are loaded onto a carbon-coated copper grid and allowed to incubate for 1 min. Excess liquid around the grid's edge is carefully removed using filter paper. Subsequently, phosphotungstic acid is applied onto the copper grid, and a 30-second incubation period follows. Again, excess liquid is removed around the grid's edge using filter paper. The grid is then air-dried at room temperature. Following the imaging instructions provided by the instrument manual, the morphology of apoVs or exosomes is observed under the transmission electron microscope, and images are captured for documentation.

Nanoparticle tracking analysis (NTA) of apoVs or exosomes

First, the sample chamber was thoroughly rinsed with deionized water to ensure cleanliness. Subsequently, instrument calibration was performed using polystyrene microspheres to ensure accuracy. Following calibration, the sample chamber was washed with phosphate-buffered saline (PBS) solution to prepare it for sample loading. The apoVs or exosomes samples were then appropriately diluted in PBS buffer before being introduced into the sample chamber. Finally, the instrument was operated according to the manufacturer's instructions for NTA analysis to measure and characterize the size distribution of apoVs or exosomes.

ApoVs biodistribution assay

ApoVs were labeled with the lipophilic fluorescent dye DiR (Solarbio) according to the manufacturer's instructions. Subsequently, they were intravenously injected via the tail vein into C57BL/6J mice with CCl4-induced liver fibrosis. After 24 h post-injection, organs such as the heart, lung, liver, spleen, and kidney were harvested. Images of these organs were captured using the IVIS imaging system.

ApoVs were labeled with PKH26 (Solarbio) following the manufacturer's instructions. Subsequently, the PKH26-labeled apoVs were intravenously injected to CCl4-induced liver fibrosis model mice. The heart, lung, liver, spleen, and kidney were harvested at the indicated times and fixed with 4% paraformaldehyde, followed by 30% sucrose. The tissues were then embedded in optimal cutting temperature (OCT) compound (SAKURA). Cryosections were prepared using a freezing microtome (Leica) and counterstained with Hoechst 33,342. To further observe uptake by specific cell types in vivo, immunofluorescent (IF) staining was performed as described above, for myofibroblast marker αSMA and macrophage marker F4/80.

Cell counting kit-8 assay

Cells were seeded in 96-well plates, and cell proliferation was assessed using a CCK-8 assay (APExBIO) according to the manufacturer's instructions. Optical density (OD) was recorded at 450 nm.

CCl4-induced liver fibrosis model and apoVs administration

Six-week-old C57BL/6J mice were obtained from GemPharmatech Co., Ltd., Nanjing. The mice were randomly assigned to different experimental groups. To establish CCl4-induced liver fibrosis model, mice received intraperitoneal injections of 0.25 μl/g of CCl4 (Sinopharm Group Chemical Reagent Co. LTD) dissolved in olive oil (Sinopharm Group Chemical Reagent Co. LTD) three times per week for 8 weeks. Mice without CCl4 treatment were used as normal control. For the administration of apoVs, a dose of 30 μg in 100 μl of sterile saline was intravenously injected into each mouse. Sterile saline injections were used as a blank control. ApoVs were injected biweekly for a total of two injections. Liver samples from the recipient mice were collected two weeks after the last injection for analysis.

DDC-induced liver fibrosis model and apoVs administration

Six-week-old C57BL/6J mice were obtained from GemPharmatech Co., Ltd., Nanjing. The mice were randomly assigned to different experimental groups. Mice fed a normal diet were used as normal control. To establish

DDC-induced liver fibrosis model, mice were fed a diet containing 0.1% DCC (Sigma) for four weeks. For the administration of apoVs, a dose of 30 μg in 100 μl of sterile saline was intravenously injected into each mouse. Sterile saline injection was used as a blank control. ApoVs were injected biweekly for a total of two injections. Liver samples from the recipient mice were collected two weeks after the last injection for analysis.

Histology and immunohistochemistry (IHC)

Liver tissues were fixed in 10% formalin (Sigma) and subsequently embedded in paraffin. Then, 5-μm-thick sections were cut from the liver tissues for further histological and immunohistochemical analyses. For Sirius Red staining, the sections were subjected to hematoxylin staining for 10 min after deparaffinization. Subsequently, the Picro Sirius Red Stain Kit (Abcam) was employed for staining, following the manufacturer's instructions. In the case of immunohistochemistry (IHC) assays, the sections were first treated with 3% H_2O_2 for 20 min and then blocked with 1% BSA in PBS for 30 min at 37 °C. Following this, the sections were incubated with the specified primary antibodies at 4 °C overnight and subsequently incubated with secondary antibodies (Jackson ImmunoResearch Laboratories, Inc.) for 30 min at 37 °C, followed by DAB staining (Dako). The primary antibodies used were as follows: rabbit anti-αSMA (Abcam, diluted 1:1000), rabbit anti-F4/80 antibody (CST, diluted 1:1000), and rabbit anti-CD206 antibody (Abcam, diluted 1:10,000).

Glucose consumption, lactate production, and LDH activity assay

Glucose consumption (Nanjing Jiancheng Bioengineering Institute), lactate production (Nanjing Jiancheng Bioengineering Institute) and LDH activity (Solarbio) were detected according to the manufacturer's instructions.

Glycolysis stress test

The real-time analysis of extracellular acidification rate (ECAR) was conducted using the Seahorse XF96 Extracellular Flux Analyzer (Seahorse Bioscience, USA) following the manufacturer's protocol. TGF-β1-induced MEFs were treated with apoVs for 3 days, and then the cells were seeded in a Seahorse XF96 culture microplate at a density of 3×10^4 cells per well overnight. ECAR was measured after the addition of glucose, oligomycin, and 2-DG.

Western blot assay

Whole lysates of cells, apoVs, or exosomes were separated on 10% SDS-polyacrylamide gels and subsequently transferred to nitrocellulose membranes (GE). These membranes were blocked with 5% BSA in 1×TBS containing 0.1% Tween-20 (TBST) for 2 h at room temperature. Afterward, the membranes were incubated with the designated primary antibodies overnight at 4 °C. Following three washes with TBST, the membranes were incubated with fluorescein-conjugated secondary antibodies for 1 h at room temperature. Fluorescent signals were detected using the LI-COR Odyssey imaging system. Primary antibodies are as follows: rabbit anti-caspase-3 antibody (CST, diluted 1:1000), rabbit anti-cleaved caspase-3 antibody (CST, diluted 1:1000), mouse anti-β-actin antibody (ABclonal, diluted 1:10000), rabbit anti-CD63 antibody (Abclonal, diluted 1:500), rabbit anti-Flotillin-2 antibody (CST, diluted 1:1000), rabbit anti-Phospho-Akt (Ser473) antibody (CST, diluted 1:1000), rabbit anti-Phospho-mTOR (Ser2448) antibody (CST, diluted 1:1000), rabbit anti-Phospho-p70 S6 Kinase (Thr389) antibody (CST, diluted 1:1000), rabbit anti-Phospho-4E-BP1 (Thr37/46) antibody (CST, diluted 1:1000), rabbit anti-PFKFB3 antibody (CST, diluted 1:1000), rabbit anti-p-SMAD2/3 antibody (Immunoway, diluted 1:500), rabbit anti-p-c-JUN antibody (Huabio, diluted 1:500), rabbit anti-SNAI1 antibody (CST, diluted 1:1000), rabbit anti-αSMA (Abcam, diluted 1:1000), rabbit anti-gamma Tubulin antibody (Abcam, diluted 1:1000). Secondary antibody is IRDye 800CW Secondary Antibodies (LI-COR).

Statistical analysis

Data are presented as mean±SD. Statistical significance was evaluated using one-way ANOVA. A P-value less than 0.05 was considered statistically significant ($^*p<0.05$, $^{**}p<0.01$, $^{***}p<0.001$).

Results

Collection and characterization of cihep-apovs

By employing a small molecule cocktail (SMC), we successfully converted fibroblasts into ciHeps, showcasing notable efficiency, convenience, and controllability [17]. This approach provides a reliable solution to the challenge of limited access to primary hepatocytes. Furthermore, our focus extended to optimizing liver fibrosis treatment utilizing either hepatocytes or ciHeps, culminating in the extraction of ciHep-derived apoVs (ciHep-apoVs) (Fig. S1). In this investigation, ciHeps were generated using the protocols outlined in our previous publications [17] (Fig. 1A). Induction of apoptosis in ciHeps was achieved through staurosporine (STS) (Fig. S2), and subsequent collection of apoVs was conducted using an optimized gradient centrifugation protocol [20] (Fig. 1B). Characterization of the collected apoVs involved assessing their morphology, size distribution, and apoptosis-related markers. Transmission electron microscopy (TEM) images revealed that ciHep-apoVs possessed the characteristic bilayer lipid membrane structure and a spherical morphology (Fig. 1C). Nanoparticle tracking analysis

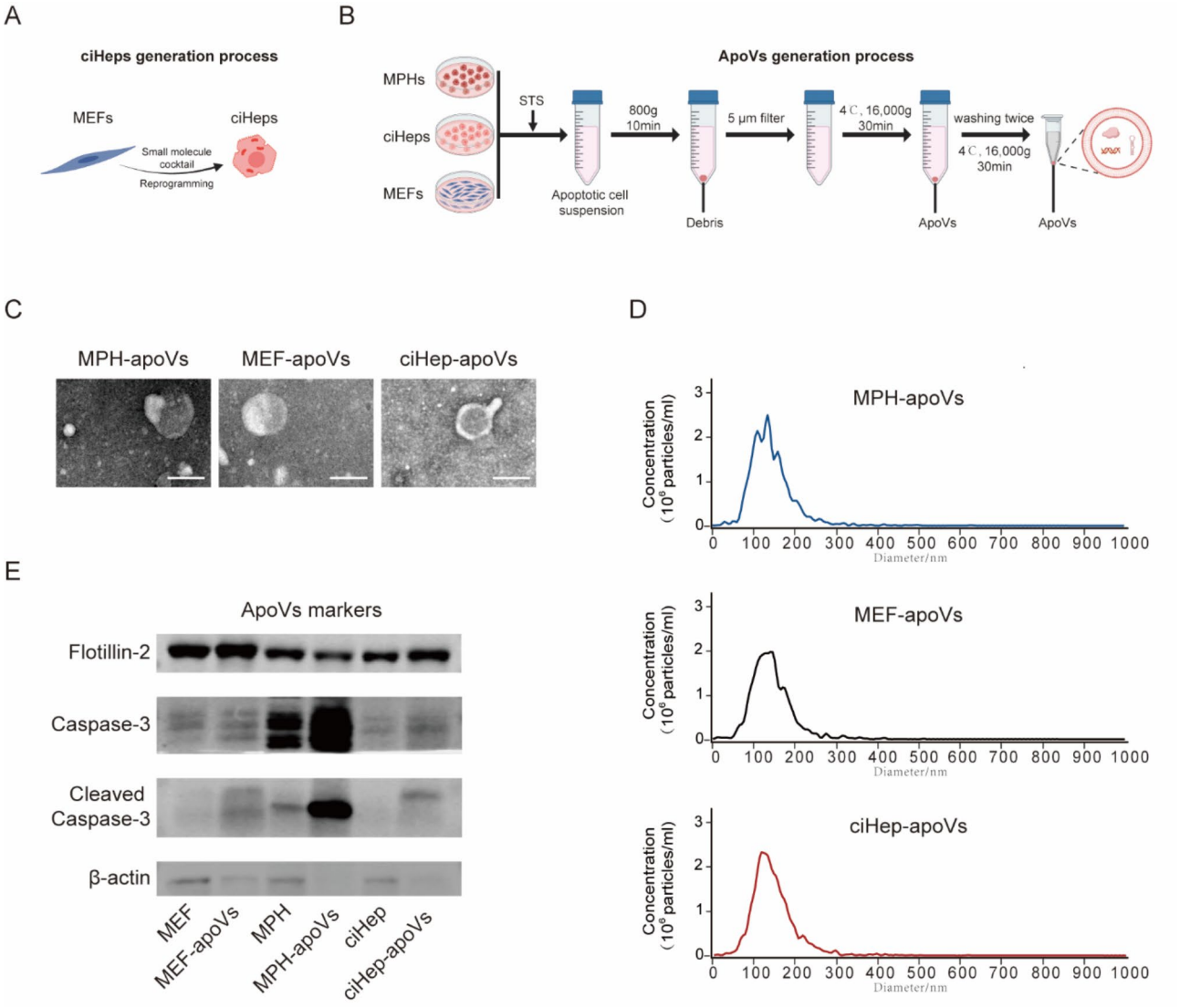

Fig. 1 Collection and Characterization of apoVs. **A**. Scheme depicting the induction of ciHeps through the application of a small molecule cocktail. **B**. Scheme outlining the process of apoVs isolation from various sources, including apoptotic ciHeps, MEFs, MPHs, etc. **C**. Representative transmission electron microscopy (TEM) images showing the morphologies of apoVs from different cell types. Scale bar: 200 nm. **D**. Nanoparticle tracking analysis (NTA) showing the size distributions of apoVs. **E**. Western blot results revealing the expression levels of Flotillin-2, Caspase-3, Cleaved Caspase-3, and β-actin in cells and apoVs

(NTA) indicated that the majority of apoVs fell within the size range of approximately 80–180 nm (Fig. 1D). Results from western blot assay confirmed the presence of the lipid raft-associated integral membrane protein Flotillin-2 within apoVs, thereby corroborating the lipid membrane structure of apoVs (Fig. 1E). Additionally, the western blot assay revealed an upregulation of Cleaved Caspase-3, an apoptosis marker, in these apoVs (Fig. 1E). The purity of the isolated apoVs was verified by the absence of β-actin expression (Fig. 1E).

In vitro assessment of anti-fibrotic potential of cihep-apovs

Extracellular vesicles encompass a diverse array of functional components and play vital roles in numerous physiological and pathological settings. While current research predominantly focuses on the therapeutic application of exosomes in liver fibrosis [21–23], we aimed to concurrently extract ciHep-derived exosomes (ciHep-exos) and identified characters of ciHep-exos (Fig. S3). Subsequently, we compared the effects of ciHep-apoVs and ciHep-exos on fibroblasts. The results indicated that ciHep-apoVs exert a stronger inhibitory effect on the growth and proliferation of fibroblasts compared to ciHep-exos, as observed in the CCK-8 assays (Fig. S4A). Moreover, ciHep-apoVs exhibited a more pronounced inhibitory effect on the expression of fibrotic marker gene *Acta2* compared to ciHep-exos (Fig. S4B). Consistent with above findings, western blot assay revealed that

ciHep-apoVs more effectively inhibited the expression of fibrotic marker α-smooth muscle actin (αSMA) (Fig. S4C). Combining the aforementioned results, ciHep-apoVs exhibited a more potent anti-fibroblast effect. Given the convenience of obtaining apoVs and their stronger inhibitory effect on fibroblasts, we focused our upcoming research on exploring the anti-fibrotic potential of ciHep-apoVs in vitro.

To ensure liver safety, antifibrotic treatments should be both hepatocyte-friendly and non-toxic. To address this, we conducted an in vitro assessment of cell viability using CCK-8 assays. The results revealed that ciHep-apoVs increased mouse primary hepatocyte (MPH) viability to a similar extent as MPH-apoVs after 24 h of treatment, while apoVs derived from mouse embryonic fibroblasts (MEF-apoVs) had a negligible effect on MPH viability (Fig. 2A). Additionally, we evaluated lactate dehydrogenase (LDH) levels, a reliable indicator of liver injury, in cultured MPHs. The results showed that ciHep-apoVs did not affect LDH release, signifying their benign influence on hepatocytes without inducing cytotoxicity (Fig. 2B).

Macrophages play a pivotal role in inflammation and liver fibrosis [24, 25]. They can be divided into pro-inflammatory (M1) and anti-inflammatory (M2) phenotypes. To assess the impact of ciHep-apoVs on macrophage polarization, peritoneal macrophages were isolated and identified by macrophage marker F4/80 staining (Fig. S5), and exposed to ciHep-apoVs. The results showed that both ciHep-apoVs and MPH-apoVs effectively downregulated the expression of the pro-inflammatory gene *Tnf-α* in macrophages after a 4-hour treatment, whereas MEF-apoVs did not produce this effect (Fig. 2C). This suppression of *Tnf-α* expression persisted for 8 h in ciHep-apoV-treated cells, concomitant with a notable increase in the expression of the anti-inflammatory gene *Arg-1* (Fig. 2D).

TGF-β is generally considered as the most potent profibrogenic cytokine, driving the activation of hepatic stellate cells (HSCs) into myofibroblasts [26]. Therefore, macrophages producing TGF-β play a key role in the progression of fibrotic diseases. *Tgf-β1* was strikingly downregulated in macrophages after 4 h of treatment with ciHep-apoVs, and this effect persisted when ciHep-apoV treatment was extended to 8 h, similar to the suppression observed with *Tnf-α* (Fig. 2C, D). Overall, ciHep-apoVs exhibited anti-inflammatory effects by reducing the expression of pro-inflammatory gene *Tnf-α* while simultaneously increasing the expression of the anti-inflammatory gene *Arg-1* in macrophages. Additionally, gene expression of prominent profibrogenic cytokine *Tgf-β1* also decreased in macrophages.

Given the pivotal role of activated hepatic stellate cells (aHSCs) in liver fibrosis [27], we aimed to explore the effects of ciHep-apoVs on these activated cells. Primary HSCs were successfully isolated and confirmed through autofluorescence detection and DESMIN expression (Fig. S6). The HSCs were then cultured for 5 days to induce activation into myofibroblasts, which were identified by the presence of star-shaped pseudopodia and cytoplasmic αSMA expression (Fig. S7). Subsequently, the myofibroblasts were then treated with ciHep-apoVs for 3 days, followed by gene expressions analysis.

The gene expression analysis revealed that ciHep-apoV treatment significantly suppressed the expression of fibrosis marker genes such as *Acta2*, *Col1a1*, *Timp1*, and *Ccn5* in myofibroblasts, while MEF-apoV treatment had no positive effect on myofibroblasts. In fact, MEF-apoV treatment led to an increase in the expression of *Timp1* in myofibroblasts (Fig. 2E). Furthermore, ciHep-apoVs effectively suppressed myofibroblast proliferation, similar to the effect of MPH-apoVs (Fig. 2F). Notably, ciHep-apoV treatment induced a morphological change in myofibroblasts, transitioning them from a star-shaped to a more rounded and oval shape, accompanied by positive Oil Red staining, indicating the restoration of lipid metabolism (Fig. 2G). The absence of αSMA staining further indicated the loss of the fibrotic cell identity (Fig. 2G).

In conclusion, our results highlight that ciHep-apoVs possess anti-inflammatory properties and effectively suppress the activation of aHSCs while being non-toxic to hepatocytes in vitro. These findings suggest their potential to mitigating liver fibrosis in vivo.

Distribution of cihep-apovs in an in vivo model of CCl4-induced liver fibrosis

We assessed the in vivo distribution of systemically administered ciHep-apoVs in different organs including the heart, lung, liver, spleen, and kidney. To track their distribution, ciHep-apoVs labeled with DiR, a fluorescent lipophilic tracer, were intravenously injected into C57BL/6 mice with CCl4-induced liver fibrosis. The imaging results showed a significant accumulation of ciHep-apoVs in the liver 24 h post-injection (Fig. 3A). This observation aligns with prior research indicating the liver's central role in organismal clearance processes [28, 29].

Furthermore, C57BL/6 mice with CCl4-induced liver fibrosis were intravenously injected with ciHep-apoVs labeled with PKH26. Tissues, including the heart, lung, liver, spleen, and kidney, were harvested at 24 h post-injection. Histological sections yielded results consistent with IVIS imaging, indicating significant accumulation of ciHep-apoVs in the liver (Fig. 3B).

In liver fibrosis diseases, hepatic stellate cells (HSCs) transition into myofibroblasts, which have the ability to uptake various EVs. Additionally, macrophages serve as the principal phagocytic cells responsible for

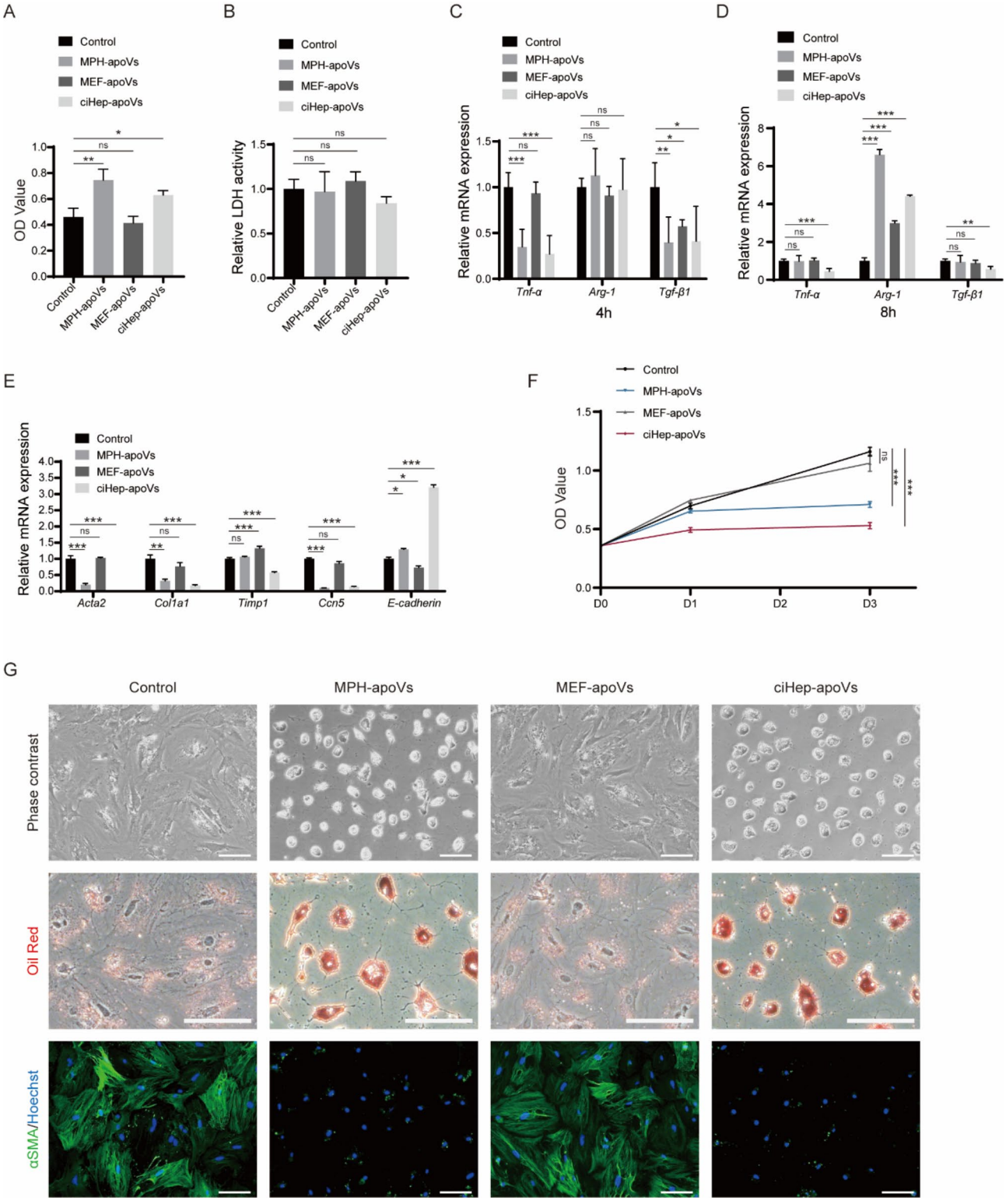

Fig. 2 Impact of apoVs on MPH protection, macrophages, and activated HSCs in vitro. **A**. Effect of apoVs on MPH viability determined by CCK-8 assay. **B**. Effect of apoVs on LDH release from MPHs. **C**-**D**. *Tnf-α*, *Arg-1*, and *Tgf-β1* expression in apoVs-treated macrophages at indicated times. **E**. Expression of fibrosis- and epithelial-related genes in apoV-treated aHSCs. **F**. Effect of apoVs on aHSCs' cell proliferation as determined by CCK-8 assay. **G**. Phase-contrast images, Oil Red staining, and αSMA immunofluorescence results in apoV-treated activated HSCs. Scale bar: 100 μm. *$p < 0.05$, **$p < 0.01$, ***$p < 0.001$

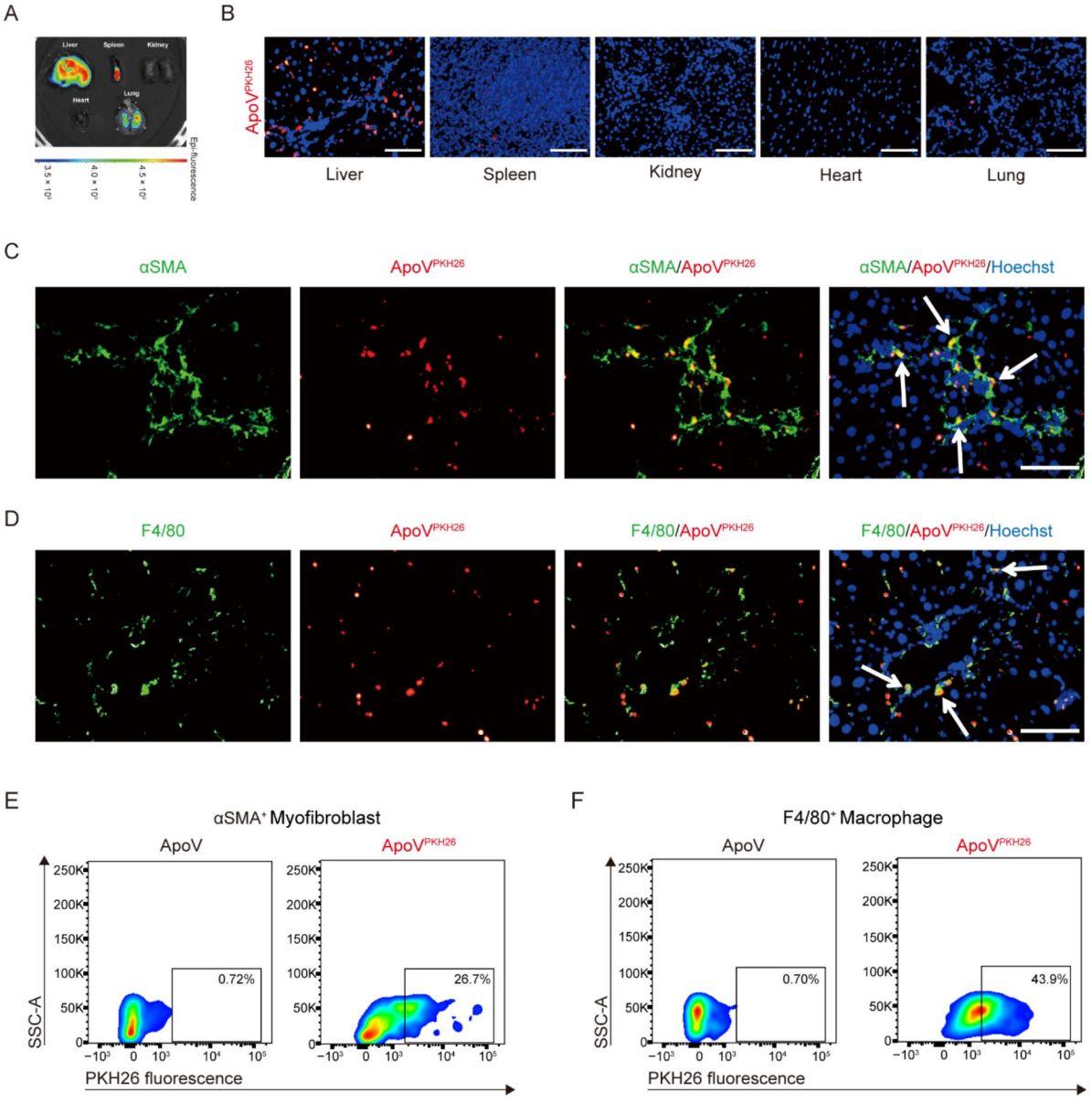

Fig. 3 Distribution and uptake of ciHep-apoVs in vivo at 24 h post-injection. **A**. Distribution of DiR-labeled ciHep-apoVs in various organs 24 h post-injection, visualized by the IVIS imaging system. **B**. Distribution of PKH26-labeled ciHep-apoVs (red) in various organs 24 h post-injection. **C**. Representative images showing ciHep-apoVs (red) being taken up by myofibroblasts (green) in the liver 24 h post-injection. **D**. Representative images showing ciHep-apoVs (red) being taken up by macrophages (green) in the liver 24 h post-injection. **E**. Flow cytometry data demonstrating the engulfment of ciHep-apoVs by myofibroblasts 24 h post-injection. **F**. Flow cytometry data demonstrating the engulfment of ciHep-apoVs by macrophages 24 h post-injection. Scale bar: 100 μm

the clearance of apoptotic cells in vivo. Given the critical roles played by the activation of HSCs and the inflammatory response of macrophages in liver fibrosis, we proceeded to investigate whether apoVs could be internalized by myofibroblasts and macrophages. Liver tissues were harvested 24 h post-injection, and liver sections were stained for αSMA, a myofibroblasts marker, and F4/80, a macrophage marker. Both myofibroblasts and macrophages were observed to actively engulf ciHep-apoVs in vivo (Fig. 3C, D). Flow cytometry further confirmed the engulfment of ciHep-apoVs by both myofibroblasts (~27%) and macrophages (~44%) (Fig. 3E, F), whereas only a small fraction of hepatocytes (~3.0%) took up the apoVs (Fig. S8).

Samples from different organs were also collected at earlier time points, either 6 or 12 h post-injection. The results further demonstrated the accumulation of ciHep-apoVs in the liver (Fig. S9A) and the uptake of

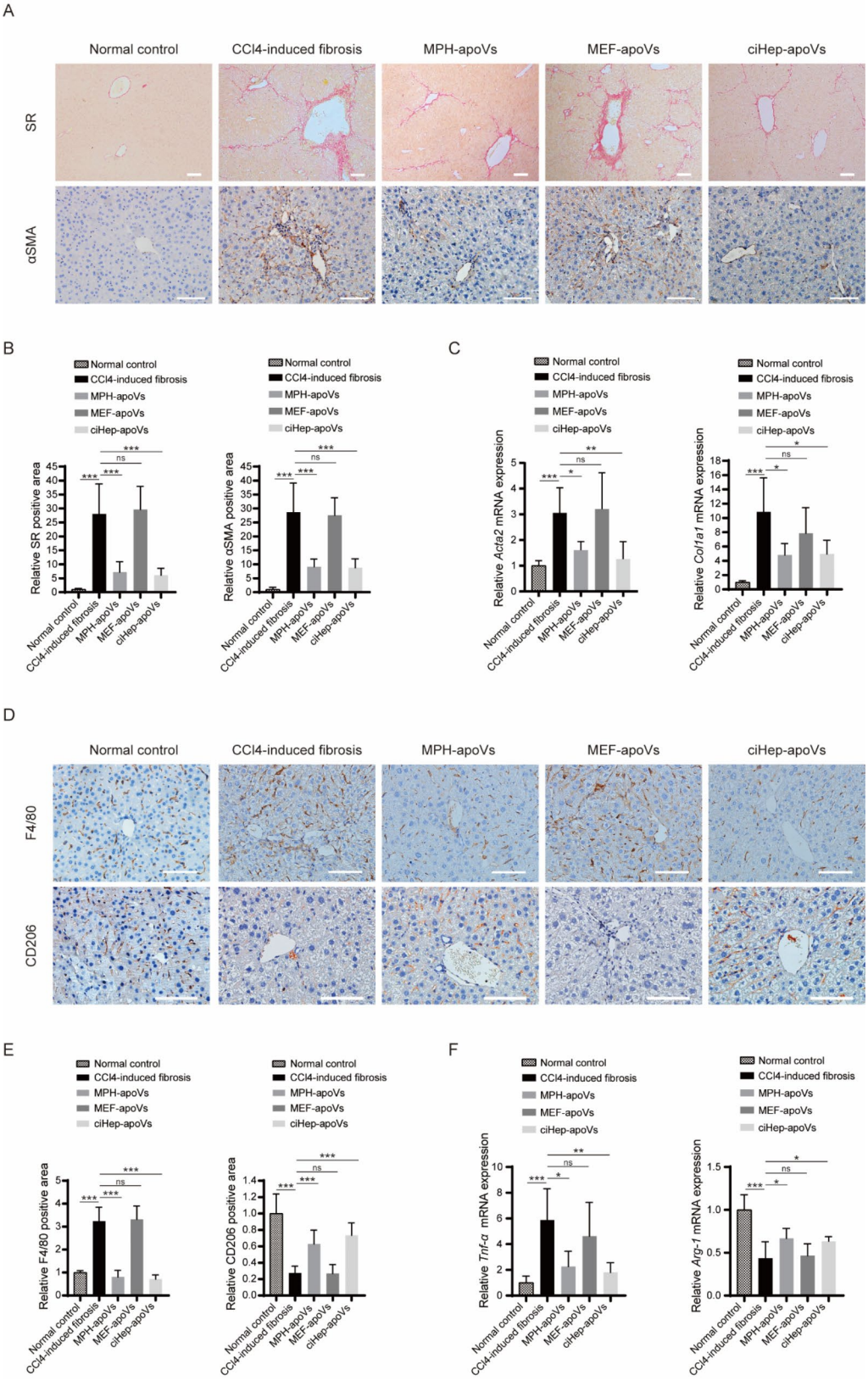

Fig. 4 (See legend on next page.)

(See figure on previous page.)

Fig. 4 Amelioration of CCl4-Induced liver fibrosis and chronic inflammation by ciHep-apoVs. **A**-**B**. Liver sections from normal control group mice and CCl4-induced fibrosis mice treated with sterile saline, MPH-apoVs, MEF-apoVs, or ciHep-apoVs ($n = 6$) show Sirius Red (SR) and αSMA staining (A) along with quantification results (B). Scale bar: 100 μm. **C**. Liver gene expression of fibrosis-related markers in normal control group mice and CCl4-induced fibrosis mice treated with sterile saline, MPH-apoVs, MEF-apoVs, or ciHep-apoVs ($n = 6$). **D**-**E**. Liver sections from normal control group mice and CCl4-induced fibrosis mice treated with sterile saline, MPH-apoVs, MEF-apoVs, or ciHep-apoVs ($n = 6$) show F4/80 and CD206 staining (D) along with quantification results (E). Scale bar: 100 μm. **F**. Liver gene expression of inflammation-related markers in normal control group mice and CCl4-induced fibrosis mice treated with sterile saline, MPH-apoVs, MEF-apoVs, or ciHep-apoVs ($n = 6$). *$p < 0.05$, **$p < 0.01$, ***$p < 0.001$

ciHep-apoVs by both myofibroblasts (Fig. S9B) and macrophages (Fig. S9C).

Alleviation of CCl4-induced liver fibrosis in vivo by cihep-apovs

Our in vitro findings demonstrated that ciHep-apoVs possessed various anti-fibrotic properties, such as enhancing MPH viability, suppressing pro-inflammatory gene expression, and promoting anti-inflammatory gene expression in macrophages. Additionally, ciHep-apoVs effectively induced a quiescent phenotype in aHSCs. Encouraged by these promising results, we proceeded to investigate the therapeutic potential of ciHep-apoVs in alleviating CCl4-induced liver fibrosis in an in vivo setting (Fig. S10).

Sirius Red (SR) staining revealed a reduction in collagen levels in the livers of mice treated with ciHep-apoVs, comparable to the effects observed with MPH-apoVs (Fig. 4A, B). This reduction was further validated by the decrease in αSMA staining levels in the ciHep-apoV-treated samples, indicating a decrease in liver fibrosis (Fig. 4A, B). Gene expression analysis provided additional support for these findings, revealing reduced expression of *Acta2* and *Col1a1* in the ciHep-apoV-treated samples (Fig. 4C).

Chronic inflammation is widely acknowledged as a key mechanism in the development of liver fibrosis. Thus, we proceeded to assess the infiltration and activation of macrophages. Positive staining for F4/80, a macrophage marker, was notably reduced in the livers of mice treated with ciHep-apoVs, similar to the effect observed with MPH-apoVs (Fig. 4D, E). Furthermore, the positive staining of CD206, a marker associated with the M2 macrophage subtype, showed an increase, providing additional evidence of improved macrophage infiltration (Fig. 4D, E). Reduced gene expression of the pro-inflammatory factor *Tnf-α*, coupled with an increase in the expression of the anti-inflammatory factor *Arg-1*, pointed towards an amelioration of chronic inflammation (Fig. 4F). Furthermore, the serum levels of ALT and AST were lower in mice treated with ciHep-apoVs, suggesting an improvement in liver function (Fig. S11). These results collectively demonstrate the effectiveness of ciHep-apoVs in alleviating CCl4-induced liver fibrosis and inflammation and improving liver function.

Validation of the anti-fibrosis effect of cihep-apovs using DDC-induced liver fibrosis

We have successfully demonstrated the efficacy of ciHep-apoVs in alleviating liver fibrosis and hepatic inflammation in a CCl4-induced liver fibrosis model. To further validate the anti-fibrotic properties of ciHep-apoVs, we employed additional fibrosis models that hold greater clinical relevance. Chronic cholestatic diseases represent a category of disorders characterized by the accumulation of hepatic bile acids, potentially leading to liver fibrosis and eventual end-stage liver disease [30, 31]. The mouse model of chronic cholestasis induced by 3,5-diethoxycarbonyl-1,4-dihydroxychollidine (DDC) feeding has been utilized for investigating the efficacy of ciHep-apoVs in treating cholestatic liver fibrosis (Fig. S12). In line with results observed in the CCl4-induced liver fibrosis model, ciHep-apoVs demonstrated a reduction in the positive staining area of hepatic fibrosis markers, such as SR and αSMA, and downregulation in the expression of fibrotic genes (Fig. 5A-C). Furthermore, improved macrophage infiltration and expression of inflammatory-related genes were observed in ciHep-apoVs treated group (Fig. 5D-F). Serum levels of ALT and AST were also lower in mice treated with ciHep-apoVs (Fig. S13).

The DDC-induced liver fibrosis model further corroborated the anti-fibrotic efficacy of ciHep-apoVs. ciHep-apoVs exhibit promising potential in ameliorating liver fibrosis induced by different etiologies.

Functional protein and miRNA enrichment of cihep-apovs

The functions of extracellular vesicles are attributed to their unique bioactive cargos, particularly proteins and miRNAs. We first investigated the proteomic content of ciHep-apoVs using LC-MS/MS analysis, with MEF-apoVs serving as a negative control. Upon comparing ciHep-apoVs to MEF-apoVs, we identified 795 differentially expressed proteins (DEPs), with 637 of them displaying significant upregulation (Fig. 6A, B). Further analysis of the subcellular localization of these DEPs showed that 20.98% were associated with mitochondrion proteins, 15.91% were cytoplasm proteins, 13.46% were nucleus proteins, 11.54% were extracellular proteins, and 11.36% were plasma membrane proteins (Fig. 6C).

We then conducted an enrichment analysis of these DEPs. Using the Gene Ontology (GO) database, we found that ciHep-apoVs exhibited an elevation in proteins involved in various functional categories, including

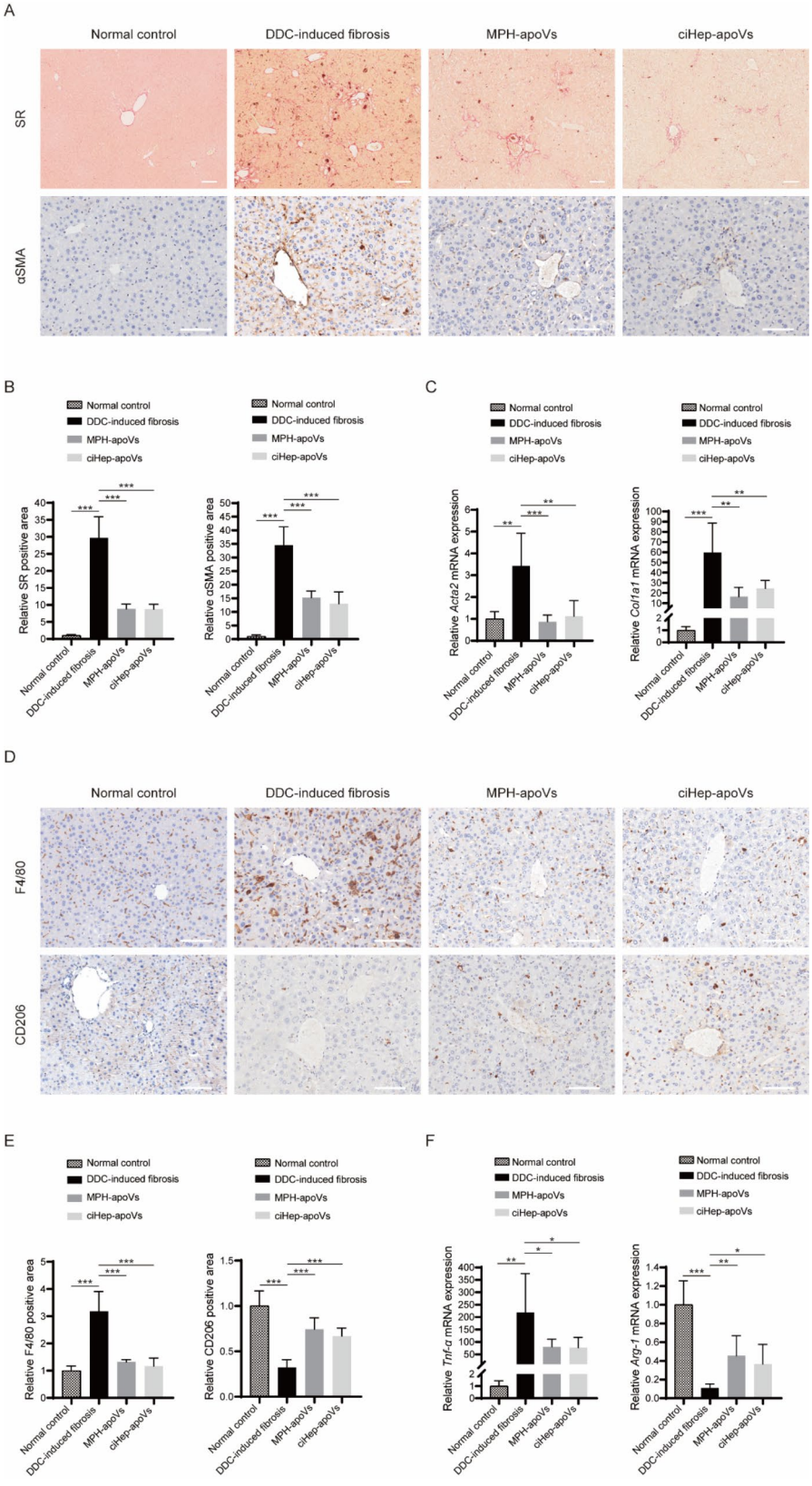

Fig. 5 (See legend on next page.)

(See figure on previous page.)

Fig. 5 Amelioration of DDC-induced liver fibrosis and chronic inflammation by ciHep-apoVs. **A**-**B**. Liver sections from normal control group mice and DDC-induced fibrosis mice treated with sterile saline, MPH-apoVs, or ciHep-apoVs ($n=6$) show Sirius Red (SR) and αSMA staining (A) along with quantification results (B). Scale bar: 100 μm. **C**. Liver gene expression of fibrosis-related markers in normal control group mice and DDC-induced fibrosis mice treated with sterile saline, MPH-apoVs, or ciHep-apoVs ($n=6$). **D**-**E**. Liver sections from normal control group mice and DDC-induced fibrosis mice treated with sterile saline, MPH-apoVs, or ciHep-apoVs ($n=6$) show F4/80 and CD206 staining (D) along with quantification results (E). Scale bar: 100 μm. **F**. Liver gene expression of inflammation-related markers in normal control group mice and DDC-induced fibrosis mice treated with sterile saline, MPH-apoVs, or ciHep-apoVs ($n=6$). $^{*}p<0.05$, $^{**}p<0.01$, $^{***}p<0.001$

metabolic processes, mitochondrion, mitochondrial membrane, oxidoreductase activity, electron carrier activity, and others (Fig. 6D). Kyoto Encyclopedia of Genes and Genomes (KEGG) pathway analysis unveiled a significant association between these upregulated proteins and metabolic pathways, oxidative phosphorylation, and the citrate cycle (TCA cycle), in line with the GO enrichment analysis (Fig. 6E). This KEGG pathway analysis also showed that the downregulated proteins in ciHep-apoVs were closely linked to focal adhesion, the PI3K-Akt signaling pathway, the MAPK signaling pathway, ECM-receptor interaction, and cytokine-cytokine receptor interaction (Fig. 6F). A network of protein-protein interactions further revealed intricate functional interactions between these DEPs (Fig. 6G). These findings collectively suggest that the proteomic profile of ciHep-apoVs is intricately associated with the regulation of metabolism, signaling transduction, and cellular behavior.

Next, we detected the miRNA expression profile of ciHep-apoVs through miRNA sequencing, utilizing MEF-apoVs as a negative control. In the comparison between ciHep-apoVs and MEF-apoVs, we identified 149 differentially expressed miRNAs (DEMs), with 73 miRNAs exhibiting upregulation in ciHep-apoVs (Fig. 7A, B). We then focused on these DEMs and carried out enrichment analysis. KEGG pathway analysis indicated that these miRNAs jointly regulated various fibrosis-related pathways, such as the PI3K-Akt signaling pathway, Notch signaling pathway, MAPK signaling pathway, Hepatitis B, and ECM-receptor interaction (Fig. 7C). To further focus on specific functional miRNAs, we conducted a comparative analysis of our data with publicly available miRNA sequencing data from another study that contrasted activated human primary HSCs with quiescent human primary HSCs [32]. Comparison with 112 downregulated miRNAs upon human HSC activation identified 14 overlapping miRNAs, and the top 7 miRNAs with the highest abundance were miR-148a-3p, let-7 g-5p, miR-26a-5p, miR-27b-3p, miR-26b-5p, miR-30c-5p, and miR-30e-5p (Fig. 7D). According to miRNA-gene network analysis of the top 7 miRNAs, these miRNAs have intricated functional interactions linked to gene networks mainly enriched in fibrosis-related pathways, such as PI3K-Akt signaling pathway, mTOR signaling pathway, Hepatitis B, MAPK signaling pathway, ErbB signaling pathway, and HIF-1 signaling pathway (Fig. 7E). It's noteworthy that some of these miRNAs, such as miR-148a-3p [33], miR-27b-3p [34], and miR-26b-5p [35] have been established as contributors to the alleviation of liver fibrosis.

Induction of multiple mechanisms by cihep-apovs synergistically contributes to the suppression of HSC activation

We have demonstrated the anti-fibrosis therapeutic potential of ciHep-apoVs and unveiled their functional bioactive cargos they carried. The enrichment analysis of proteomic profile revealed that ciHep-apoVs possessed an abundance of proteins associated with metabolic pathways, oxidative phosphorylation, and the citrate cycle (TCA cycle). Importantly, cell metabolism, particularly increased glycolysis, plays a pivotal role in the activation of HSCs, driving their transdifferentiation into myofibroblasts [36, 37].

Our experiments showed that ciHep-apoVs led to a reduction in glucose consumption, lactate production, and the gene expression of the glycolytic enzyme *Pfkfb3* in treated myofibroblasts (Fig. 8A-C). Elevated PFKFB3 expression is a characteristic feature of HSC activation, and its reduction can effectively decrease myofibroblast proliferation and activation [38]. To further validate these results, we conducted experiments using MEFs activated with TGF-β1 to mimic the activated HSCs state (Fig. S14). TGF-β1-induced MEFs under ciHep-apoV treatment exhibited analogous changes in glycolysis and *Pfkfb3* gene expression, similar to the responses observed in aHSCs (Fig. S15). Measurement of the extracellular acidification rate (ECAR) further confirmed a significant decrease in TGF-β1-induced MEFs following treatment with ciHep-apoVs (Fig. 8D). Furthermore, ciHep-apoV treatment resulted in a significant reduction in fibrosis-related genes and an upregulation of the epithelial marker *E-cadherin* (Fig. 8E).

Enrichment analysis of both proteomic and miRNA profiles indicated that ciHep-apoVs may regulate several key signaling pathways, including the PI3K-Akt signaling pathway, MAPK signaling pathway, ECM-receptor interaction, and others, likely through the synergistic effects of their bioactive molecules. The PI3K/Akt/mTOR signaling pathway plays a crucial role in liver fibrosis, as its activation leads to increased HSC activation and proliferation [39–41]. Our experiments revealed that ciHep-apoVs effectively downregulated phosphorylation levels of key targets within the PI3K/Akt/mTOR signaling pathway,

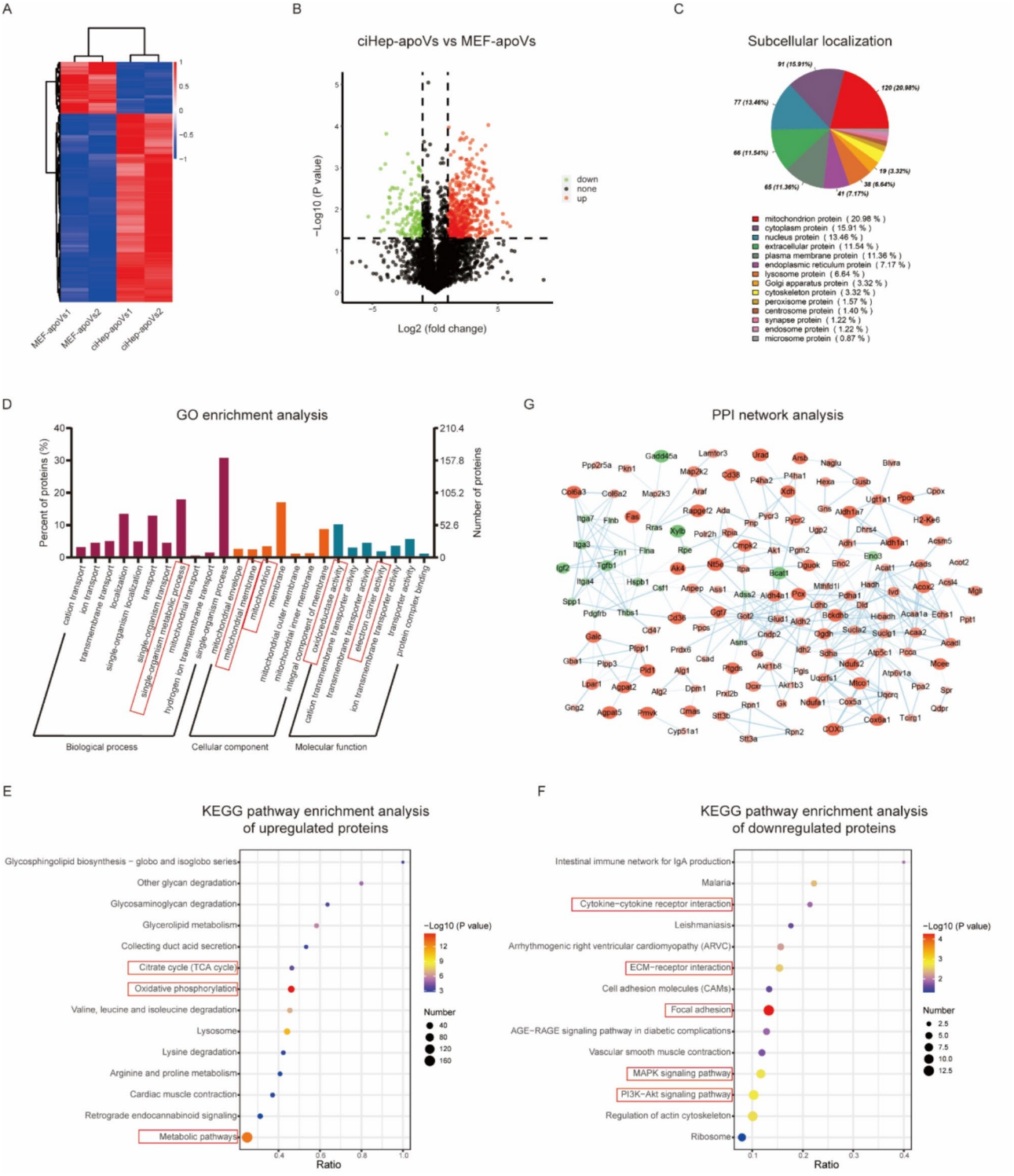

Fig. 6 Proteomic analysis demonstrating enrichment of various functional proteins in ciHep-apoVs. **A**. Heatmap of differentially expressed proteins (DEPs) between ciHep-apoVs and MEF-apoVs. **B**. Volcano plot showing DEPs in ciHep-apoVs compared to MEF-apoVs. The red and green dots indicate upregulated and downregulated proteins, respectively. **C**. Subcellular localization of DEPs in ciHep-apoVs compared to MEF-apoVs. **D**. GO enrichment analysis of DEPs in ciHep-apoVs compared to MEF-apoVs, categorized into 'Biological process', 'Cellular component' and 'Molecular function'. **E**-**F**. KEGG pathway enrichment analysis of upregulated (E) and downregulated (F) proteins in ciHep-apoVs compared to MEF-apoVs. G. Protein-protein interaction (PPI) network analysis of the DEPs in ciHep-apoVs compared to MEF-apoVs

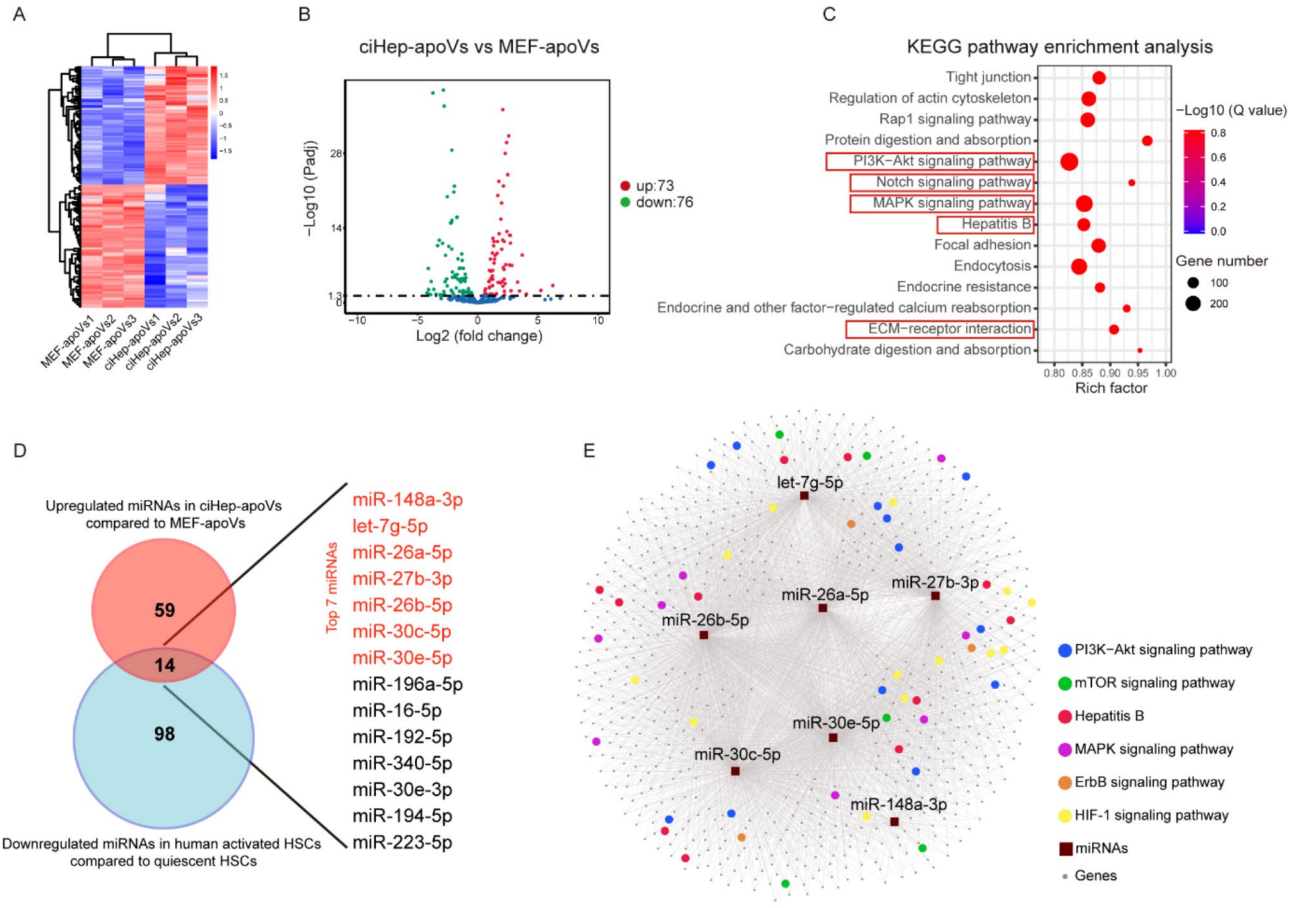

Fig. 7 miRNA sequencing analysis demonstrating enrichment of various functional miRNAs in ciHep-apoVs. **A**. Heatmap of differentially expressed miRNAs (DEMs) between ciHep-apoVs and MEF-apoVs. **B**. Volcano plot showing DEMs in ciHep-apoVs compared to MEF-apoVs. The red and green dots indicate upregulated and downregulated miRNAs, respectively. **C**. KEGG pathway enrichment analysis showing that DEMs were highly related to fibrosis-related pathways. **D**. A Venn diagram of miRNA-sequencing data for "upregulated miRNAs in ciHep-apoVs compared to MEF-apoVs" and "downregulated miRNAs in human activated HSCs compared to quiescent HSCs" identified 14 overlapping miRNAs and the top 7 miRNAs with the highest abundance. **E**. miRNA-gene network analysis and KEGG pathway enrichment analysis of the top 7 miRNAs

including AKT, mTOR, S6K, 4E-BP1, as well as the expression of PFKFB3 (Fig. 8F).

Moreover, it's worth noting that activation of the PI3K/Akt/mTOR pathway also contributes to epithelial-to-mesenchymal transition (EMT) cascade [42], another hallmark of liver fibrosis. Western blot analysis showed that ciHep-apoV treatment significantly suppressed the levels of αSMA, a marker of activated myofibroblasts, and SNAI1, a key regulator in the EMT signaling pathway, further highlighting their potential anti-fibrotic effects (Fig. 8F).

Additionally, it is well known that SMAD2/3 and transcription factor activator protein-1 (AP-1) are major mediators of the fibrogenic response and EMT. Western blot results also showed that ciHep-apoV treatment significantly suppressed the levels of p-SMAD2/3 and p-c-JUN, a component of AP-1 (Fig. S16). The findings were further validated in primary aHSCs, confirming the effects of ciHep-apoVs on the PI3K-Akt signaling pathway, PFKFB3, and EMT signaling pathway (Fig. S17).

To ascertain whether ciHep-apoVs function via inhibition of glycolysis, the PI3K/AKT/mTOR signaling pathway, and EMT to suppress the activity of activated myofibroblasts, we treated activated MEFs with specific inhibitors targeting AKT, mTOR, TGFβ1, and glycolysis. CCK-8 assay results indicated that inhibition of AKT, mTOR, EMT, or glycolysis effectively restrained the growth and proliferation of activated fibroblasts (Fig. 8G). Similarly, individual administration of these inhibitors markedly reduced the gene expression of *Acta2* (Fig. 8H).

Western blot analyses confirmed that AKT or mTOR inhibition not only disrupted the PI3K/AKT/mTOR signaling axis but also attenuated the expression levels of SNAI1 and αSMA, indicative of suppressed fibroblast activity (Fig. 8I). Inhibition of EMT via TGF-β1 inhibitor significantly suppressed SNAI1 and αSMA expression

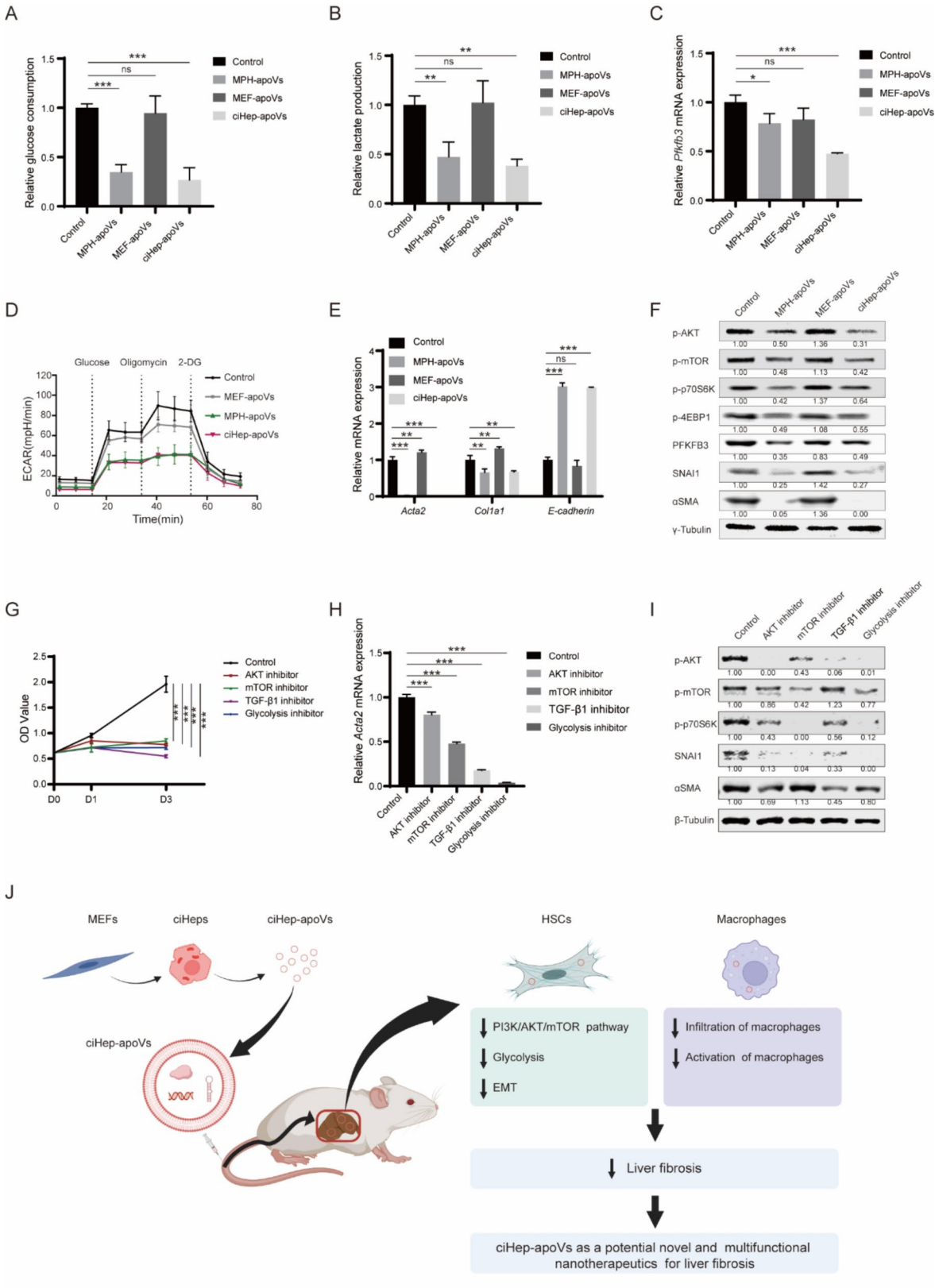

Fig. 8 (See legend on next page.)

(See figure on previous page.)

Fig. 8 The impact of ciHep-apoV treatment on the PI3K/Akt/mTOR signaling pathway, SNAI1, and glycolysis in activated HSCs and TGF-β1-induced MEFs. **A**-**B**. ciHep-apoVs treatment for 3 days reduces glucose consumption and lactate production in activated HSCs. **C**. The expression of the glycolysis enzyme *Pfkfb3* was decreased in aHSCs treated with ciHep-apoVs for 3 days. **D**. ECAR of TGF-β1-induced MEFs was decreased with ciHep-apoVs treatment for 3 days. **E**. Gene expressions of fibrosis-related genes, *Acta2*, *Col1a1*, and *E-cadherin*, were measured in TGF-β1-induced MEFs under ciHep-apoV treatment for 3 days. **F**. Western blot assay confirmed the suppression of the PI3K/Akt/mTOR signaling pathway, PFKFB3, and SNAI1 in TGF-β1-induced MEFs treated with ciHep-apoVs. **G**. CCK-8 assay showing the effects of inhibitors targeting AKT, mTOR, TGF-β1, and glycolysis on growth and proliferation of activated fibroblasts. AKT inhibitor was AKT inhibitor VIII. mTOR inhibitor was Torkinib. TGF-β1 inhibitor was A83-01. Glycolysis inhibitor was 2-DG. **H**. Gene expressions of *Acta2* of activated fibroblasts with inhibitors targeting AKT, mTOR, TGF-β1, and glycolysis. AKT inhibitor was AKT inhibitor VIII. mTOR inhibitor was Torkinib. TGF-β1 inhibitor was A83-01. Glycolysis inhibitor was 2-DG. **I**. Western blot assay showing the suppression of PI3K/Akt/mTOR signaling pathway, SNAI1, and αSMA in activated fibroblasts under inhibitors targeting AKT, mTOR, TGF-β1, and glycolysis. AKT inhibitor was AKT inhibitor VIII. mTOR inhibitor was Torkinib. TGF-β1 inhibitor was A83-01. Glycolysis inhibitor was 2-DG. **J**. Schematic diagram illustrating the anti-fibrotic effects of ciHep-apoVs and the mechanisms. $^{*}p < 0.05$, $^{**}p < 0.01$, $^{***}p < 0.001$

levels, underscoring the efficacy of EMT inhibition in curtailing activated fibroblast activity (Fig. 8I). Glycolysis inhibition not only decreased SNAI1 and αSMA expression but also attenuated the PI3K/AKT/mTOR signaling pathway, highlighting glycolysis inhibition as a potent strategy against activated fibroblasts (Fig. 8I).

Taken together, these results demonstrated that ciHep-apoVs have the capacity to concomitantly suppress the PI3K/AKT/mTOR signaling pathway, EMT, and glycolysis, effectively curbing fibroblasts activation through the synergistic modulation of these key targets.

Upon comprehensive analysis of both in vitro and in vivo experimental results, ciHep-apoVs have displayed a significant inhibitory effect on key mediators to suppress activated hepatic stellate cell (aHSC) activity. The capability of ciHep-apoVs to modulate immunological properties and attenuate inflammatory responses also contributes to the anti-fibrotic effects. Thus, ciHep-apoVs present a promising novel therapeutic avenue for liver fibrosis (Fig. 8J).

Discussion

Liver fibrosis is a serious condition requiring effective therapeutic approaches, and the application of ciHep-apoV offers new opportunities for treatment. Our study demonstrates the effectiveness of ciHep-apoVs in alleviating liver fibrosis, presenting advantages over traditional cell transplantation such as ease of use, reduced risk, and minimal immune rejection [43]. These findings highlight ciHep-apoV as a promising therapeutic strategy for liver fibrosis.

A growing body of evidence suggests that extracellular vesicles (EVs) play a crucial role in modulating recipient cells by delivering a wide array of bioactive cargos [44, 45]. While previous studies have mainly focused on stem cell-derived exosomes in liver fibrosis [21–23], our study concentrated on apoVs derived from specific organ-source cells. The effects of EVs vary depending on their unique molecular cargos. Although the differences between exosomes and apoVs are not fully understood, our results revealed that ciHep-apoVs exhibit unique advantages in inhibiting fibroblast activity compared to ciHep-exos, indicating the potential of organ-specific functional cells in treating specific organ diseases.

Interestingly, ciHep-apoVs exhibit antifibrotic effects similar to MPH-apoVs, suggesting that fibroblast-derived ciHeps could replace MPH to some extent. Given the limited availability of primary hepatocytes and the shortage of MPH-apoVs, using small molecules to induce fibroblast reprogramming to obtain ciHeps is a promising way to overcome the bottleneck of primary hepatocyte shortage. Fibroblast-derived ciHeps provide a sufficient alternative source of hepatocytes, ensuring a reliable supply of ciHep-apoVs, enhancing the potential for future clinical applications. This approach also holds promise for treating other liver diseases and fibrosis in other organs.

The mechanisms by which ciHep-apoVs reduce liver fibrosis are multifaceted. Multi-omics analysis, encompassing proteomic and miRNA profiles, revealed that ciHep-apoVs are enriched with functional molecules that profoundly impact metabolism regulation, signaling transduction, ECM-receptor interaction, cytokine-cytokine receptor interaction, and more. These various functional cargos form the basis of the anti-fibrotic effect of ciHep-apoVs.

Firstly, ciHep-apoVs promote the transition of macrophages from an M1 to M2 phenotype, effectively mitigating liver inflammation. While some reports show that M2 macrophages can produce TGF-β1 and promote fibrosis [46, 47], other studies reveal that they inhibit fibrosis by secreting anti-inflammatory factors that mitigate HSC proliferation and fibrogenesis during liver injury [48, 49]. In our research show that ciHep-apoVs reduce the expression of the pro-inflammatory gene *Tnf-α* and increase the expression of the anti-inflammatory gene *Arg-1*. They also decrease the expression of the pro-fibrotic gene *Tgf-β1*, suggesting that ciHep-apoVs facilitate the polarization of macrophages towards M2 subtypes that do not express *Tgf-β1*, allowing the anti-inflammatory and tissue repair functions of M2 macrophages to predominate.

Secondly, ciHep-apoVs inhibit HSC activation and proliferation, crucial aspects of liver fibrosis pathogenesis. Upon injection, ciHep-apoVs localize primarily in the liver, where they are internalized by liver Kupffer cells

(KCs) and activated HSCs. This synergy reduces inflammation and inhibits HSC activation, ultimately reducing liver fibrosis.

The synergistic effect of ciHep-apoVs is another noteworthy aspect of our study. We observed that ciHep-apoVs are notably enriched in proteins associated with mitochondrion and oxidative phosphorylation. This regulation of metabolic processes plays a key role in the anti-fibrotic potential of ciHep-apoVs. Moreover, ciHep-apoVs orchestrate the modulation of numerous signaling pathways and processes through their cargo molecules. By targeting HSC activation and macrophage polarization, ciHep-apoVs offer a comprehensive approach to liver fibrosis treatment.

While our study has yielded promising results, further investigation is paramount to gain a comprehensive understanding of the potential of ciHep-apoV therapy for liver fibrosis and its practical application. To ensure the success of ciHep-apoV therapy, several critical issues must be addressed: (1) the exploration of methods for generating human ciHep-apoVs, (2) the standardization and optimization of ciHep-apoVs production, (3) ensuring an adequate supply of ciHep-apoVs for treatment, (4) determining the most effective route of delivery, such as intravenous or intraperitoneal injection, and (5) conducting thorough evaluations of the safety and efficacy of ciHep-apoVs in preclinical and clinical trials.

In summary, our study not only demonstrates the promising therapeutic potential of ciHep-apoVs as multifunctional nanotherapeutics for liver fibrosis but also illuminates potential therapeutic strategies for other liver diseases and fibrosis in other organs. This research serves as a foundational step for future investigations into the multifaceted therapeutic capabilities of apoVs and their application in diverse clinical settings.

Conclusions

This study addresses the significant global health issue of liver fibrosis, which currently has limited effective treatment options. Chemical-induced hepatocyte-like cells (ciHeps) have potential for cell transplantation therapy, yet come with associated risks. Our research explores ciHep-derived apoptotic vesicles (ciHep-apoVs) as a promising alternative for liver fibrosis treatment. We found that ciHep-apoVs inhibit activated hepatic stellate cells (aHSCs), promote anti-inflammatory macrophage phenotypes, and enhance hepatocyte survival, effectively reducing liver inflammation and fibrosis. Proteomic and miRNA analyses reveal that ciHep-apoVs are enriched with molecules regulating metabolism, signaling, and ECM-receptor interactions. Mechanistically, ciHep-apoVs suppress aHSCs by inhibiting glycolysis, the PI3K/AKT/mTOR pathway, and epithelial-to-mesenchymal transition (EMT) cascades. Our findings propose ciHep-apoVs as multifunctional nanotherapeutics for treating liver fibrosis, offering new avenues for the management of fibrotic diseases.

Abbreviations

aHSCs	Activated hepatic stellate cells
AP-1	Activator protein-1
ApoVs	Apoptotic vesicles
αSMA	α-smooth muscle actin
CCK8	Cell Counting Kit-8
ciHeps	Chemical-induced hepatocyte-like cells
ciHep-apoVs	ciHep-derived apoptotic vesicles
ciHep-exos	ciHep-derived exosomes
DDC	3,5-diethoxycarbonyl-1,4-dihydroxychollidine
DEMs	Differentially expressed miRNAs
DEPs	Differentially expressed proteins
ECAR	Extracellular acidification rate
EMT	Epithelial-to-mesenchymal transition
EV	Extracellular vesicle
GO	Gene Ontology
HSCs	Hepatic stellate cells
KEGG	Kyoto Encyclopedia of Genes and Genomes
LDH	Lactate dehydrogenase
MEFs	Mouse embryonic fibroblasts
MEF-apoVs	MEF-derived apoptotic vesicles
MPHs	Mouse primary hepatocytes
MPH-apoVs	MPH-derived apoptotic vesicles
MVs	Microvesicles
NTA	Nanoparticle tracking analysis
RT-qPCR	Real-time fluorescent quantitative polymerase chain reaction
SMC	Small molecule cocktail
SR	Sirius Red
STS	Staurosporine
TEM	Transmission electron microscopy

Supplementary Information

The online version contains supplementary material available at https://doi.org/10.1186/s12951-024-02824-7.

Supplementary Material 1

Acknowledgements

We extend our thanks to the members of the International Cooperation Laboratory on Signal Transduction, especially Linna Guo, Dan Cao for excellent technical assistance.

Author contributions

Z.Z., X.C., K.T., X.W., X.Z., J.Z. and W.Z. conducted the experiments, Z.Z., X.C., analyzed the data. Z.Z. wrote the manuscript. P.Z. designed the project and revised the manuscript. P.Z. and H.W. supervised the research.All authors reviewed the manuscript.

Funding

This work was supported by the Major National Science and Technology Projects (2018ZX10302207), Project of State Key Laboratory of Systems Medicine for Cancer (KF2410), and Project of Naval Medical University (2023MS015).

Data availability

All data generated or used during the study are available from the corresponding author upon reasonable request.

Declarations

Competing interests

The authors declare no competing interests.

Author details
[1]National Center for Liver Cancer, Naval Medical University, 366 Qianju Road, Shanghai 201805, China
[2]International Cooperation Laboratory on Signal Transduction, Eastern Hepatobiliary Surgery Institute, Naval Medical University, Shanghai 200438, China
[3]Fudan University Shanghai Cancer Center, Department of Oncology, Shanghai Medical College, Fudan University, Shanghai 200032, China
[4]Institute of Metabolism & Integrative Biology, Fudan University, Shanghai 200438, China

Received: 24 June 2024 / Accepted: 31 August 2024
Published online: 05 September 2024

References

1. Poynard T, Mathurin P, Lai CL, Guyader D, Poupon R, Tainturier MH, et al. A comparison of fibrosis progression in chronic liver diseases. J Hepatol. 2003;38:257–65.
2. Asrani SK, Devarbhavi H, Eaton J, Kamath PS. Burden of liver diseases in the world. J Hepatol. 2019;70:151–71.
3. Khan S, Mahgoub S, Fallatah N, Lalor PF, Newsome PN. Liver Disease and Cell Therapy: advances made and remaining challenges. Stem Cells. 2023;41:739–61.
4. Khan S, Khan RS, Newsome PN. Cell therapy for Liver Disease: from Promise to reality. Semin Liver Dis. 2020;40:411–26.
5. Guo C, Guo G, Zhou X, Chen Y, Han Z, Yang C, et al. Long-term outcomes of autologous peripheral blood stem cell transplantation in patients with cirrhosis. Clin Gastroenterol Hepatol. 2019;17:1175–82. e2.
6. Shao H, Im H, Castro CM, Breakefield X, Weissleder R, Lee H. New Technologies for Analysis of Extracellular Vesicles. Chem Rev. 2018;118:1917–50.
7. van Niel G, D'Angelo G, Raposo G. Shedding light on the cell biology of extracellular vesicles. Nat Rev Mol Cell Biol. 2018;19:213–28.
8. Brock CK, Wallin ST, Ruiz OE, Samms KM, Mandal A, Sumner EA, et al. Stem cell proliferation is induced by apoptotic bodies from dying cells during epithelial tissue maintenance. Nat Commun. 2019;10:1044.
9. Liu D, Kou X, Chen C, Liu S, Liu Y, Yu W, et al. Circulating apoptotic bodies maintain mesenchymal stem cell homeostasis and ameliorate osteopenia via transferring multiple cellular factors. Cell Res. 2018;28:918–33.
10. Pavlyukov MS, Yu H, Bastola S, Minata M, Shender VO, Lee Y, et al. Apoptotic cell-derived extracellular vesicles promote malignancy of Glioblastoma Via Intercellular transfer of splicing factors. Cancer Cell. 2018;34:119–35. e10.
11. Kalluri R, LeBleu VS. The biology, function, and biomedical applications of exosomes. Science. 2020;367.
12. Phan TK, Poon IK, Atkin-Smith GK. Detection and isolation of apoptotic bodies to high purity. J Vis Exp. 2018.
13. Atkin-Smith GK, Poon IKH. Disassembly of the dying: mechanisms and functions. Trends Cell Biol. 2017;27:151–62.
14. Xu X, Lai Y, Hua ZC. Apoptosis and apoptotic body: disease message and therapeutic target potentials. Biosci Rep. 2019;39.
15. Kowal J, Arras G, Colombo M, Jouve M, Morath JP, Primdal-Bengtson B, et al. Proteomic comparison defines novel markers to characterize heterogeneous populations of extracellular vesicle subtypes. Proc Natl Acad Sci U S A. 2016;113:E968–77.
16. Phan TK, Ozkocak DC, Poon IKH. Unleashing the therapeutic potential of apoptotic bodies. Biochem Soc Trans. 2020;48:2079–88.
17. Zhong Z, Du J, Zhu X, Guan L, Hu Y, Zhang P et al. Highly efficient conversion of mouse fibroblasts into functional hepatic cells under chemical induction. J Mol Cell Biol. 2023.
18. Li WC, Ralphs KL, Tosh D. Isolation and culture of adult mouse hepatocytes. Methods Mol Biol. 2010;633:185–96.
19. Mederacke I, Dapito DH, Affo S, Uchinami H, Schwabe RF. High-yield and high-purity isolation of hepatic stellate cells from normal and fibrotic mouse livers. Nat Protoc. 2015;10:305–15.
20. Liu H, Liu S, Qiu X, Yang X, Bao L, Pu F, et al. Donor MSCs release apoptotic bodies to improve myocardial infarction via autophagy regulation in recipient cells. Autophagy. 2020;16:2140–55.
21. Povero D, Pinatel EM, Leszczynska A, Goyal NP, Nishio T, Kim J et al. Human induced pluripotent stem cell-derived extracellular vesicles reduce hepatic stellate cell activation and liver fibrosis. JCI Insight. 2019;5.
22. Li T, Yan Y, Wang B, Qian H, Zhang X, Shen L, et al. Exosomes derived from human umbilical cord mesenchymal stem cells alleviate liver fibrosis. Stem Cells Dev. 2013;22:845–54.
23. Bruno S, Pasquino C, Herrera Sanchez MB, Tapparo M, Figliolini F, Grange C, et al. HLSC-Derived extracellular vesicles attenuate liver fibrosis and inflammation in a murine model of non-alcoholic steatohepatitis. Mol Ther. 2020;28:479–89.
24. Rao J, Wang H, Ni M, Wang Z, Wang Z, Wei S, et al. FSTL1 promotes liver fibrosis by reprogramming macrophage function through modulating the intracellular function of PKM2. Gut. 2022;71:2539–50.
25. Baeck C, Wehr A, Karlmark KR, Heymann F, Vucur M, Gassler N, et al. Pharmacological inhibition of the chemokine CCL2 (MCP-1) diminishes liver macrophage infiltration and steatohepatitis in chronic hepatic injury. Gut. 2012;61:416–26.
26. Tsuchida T, Friedman SL. Mechanisms of hepatic stellate cell activation. Nat Rev Gastroenterol Hepatol. 2017;14:397–411.
27. Kisseleva T, Brenner D. Molecular and cellular mechanisms of liver fibrosis and its regression. Nat Rev Gastroenterol Hepatol. 2021;18:151–66.
28. Poon W, Zhang YN, Ouyang B, Kingston BR, Wu JLY, Wilhelm S, et al. Elimination pathways of nanoparticles. ACS Nano. 2019;13:5785–98.
29. Tsoi KM, MacParland SA, Ma XZ, Spetzler VN, Echeverri J, Ouyang B, et al. Mechanism of hard-nanomaterial clearance by the liver. Nat Mater. 2016;15:1212–21.
30. Ibrahim SH, Kamath BM, Loomes KM, Karpen SJ. Cholestatic liver diseases of genetic etiology: advances and controversies. Hepatology. 2022;75:1627–46.
31. Petrov PD, Soluyanova P, Sanchez-Campos S, Castell JV, Jover R. Molecular mechanisms of hepatotoxic cholestasis by clavulanic acid: role of NRF2 and FXR pathways. Food Chem Toxicol. 2021;158:112664.
32. Liu X, Ma H, Wu R, Wang H, Xu H, Li S et al. Identification of liver fibrosis-related MicroRNAs in human primary hepatic stellate cells using high-throughput sequencing. Genes (Basel). 2022;13.
33. Xiong J, Ni J, Chen C, Wang K. miR–148a–3p regulates alcoholic liver fibrosis through targeting ERBB3. Int J Mol Med. 2020;46:1003–12.
34. Cheng F, Yang F, Wang Y, Zhou J, Qian H, Yan Y. Mesenchymal stem cell-derived exosomal miR-27b-3p alleviates liver fibrosis via downregulating YAP/LOXL2 pathway. J Nanobiotechnol. 2023;21:195.
35. Yang L, Dong C, Yang J, Yang L, Chang N, Qi C, et al. MicroRNA-26b-5p inhibits mouse liver fibrogenesis and angiogenesis by targeting PDGF receptor-Beta. Mol Ther Nucleic Acids. 2019;16:206–17.
36. Gajendiran P, Vega LI, Itoh K, Sesaki H, Vakili MR, Lavasanifar A, et al. Elevated mitochondrial activity distinguishes fibrogenic hepatic stellate cells and sensitizes for selective inhibition by mitotropic doxorubicin. J Cell Mol Med. 2018;22:2210–9.
37. Chen Y, Choi SS, Michelotti GA, Chan IS, Swiderska-Syn M, Karaca GF, et al. Hedgehog controls hepatic stellate cell fate by regulating metabolism. Gastroenterology. 2012;143:1319–29. e11.
38. Mejias M, Gallego J, Naranjo-Suarez S, Ramirez M, Pell N, Manzano A, et al. CPEB4 increases expression of PFKFB3 to Induce Glycolysis and activate mouse and human hepatic stellate cells, promoting liver fibrosis. Gastroenterology. 2020;159:273–88.
39. Zhan Z, Chen Y, Duan Y, Li L, Mew K, Hu P, et al. Identification of key genes, pathways and potential therapeutic agents for liver fibrosis using an integrated bioinformatics analysis. PeerJ. 2019;7:e6645.
40. Urtasun R, Lopategi A, George J, Leung TM, Lu Y, Wang X, et al. Osteopontin, an oxidant stress sensitive cytokine, up-regulates collagen-I via integrin alpha(V)beta(3) engagement and PI3K/pAkt/NFkappaB signaling. Hepatology. 2012;55:594–608.
41. Li J, Deng X, Wang S, Jiang Q, Xu K. Resolvin D1 attenuates CCl4 Induced Liver Fibrosis by inhibiting autophagy-mediated HSC activation via AKT/mTOR pathway. Front Pharmacol. 2021;12:792414.
42. Zheng L, Yang S, Xu R, Yang Y, Quan J, Lin Z et al. NQO1 drives glioblastoma cell aggressiveness through EMT induction via the PI3K/Akt/mTOR/Snail pathway. Int J Oncol. 2023;63.
43. Lou P, Liu S, Xu X, Pan C, Lu Y, Liu J. Extracellular vesicle-based therapeutics for the regeneration of chronic wounds: current knowledge and future perspectives. Acta Biomater. 2021;119:42–56.
44. Wang Y, Zhao M, Liu S, Guo J, Lu Y, Cheng J, et al. Macrophage-derived extracellular vesicles: diverse mediators of pathology and therapeutics in multiple diseases. Cell Death Dis. 2020;11:924.
45. Dang CP, Leelahavanichkul A. Over-expression of miR-223 induces M2 macrophage through glycolysis alteration and attenuates LPS-induced sepsis mouse model, the cell-based therapy in sepsis. PLoS ONE. 2020;15:e0236038.

46. Xue J, Xiao T, Wei S, Sun J, Zou Z, Shi M, et al. miR-21-regulated M2 polarization of macrophage is involved in arsenicosis-induced hepatic fibrosis through the activation of hepatic stellate cells. J Cell Physiol. 2021;236:6025–41.
47. Zheng Y, Ji S, Li X, Wen L. Qijia rougan formula ameliorates ECM deposition in hepatic fibrosis by regulating the JAK1/STAT6-microRNA-23a feedback loop in macrophage M2 polarization. Biomed Pharmacother. 2023;168.
48. Fang W, Deng Z, Benadjaoud F, Yang C, Shi G-P. Cathepsin B deficiency ameliorates liver lipid deposition, inflammatory cell infiltration, and fibrosis after diet-induced nonalcoholic steatohepatitis. Translational Res. 2020;222:28–40.
49. Luo X-Y, Meng X-J, Cao D-C, Wang W, Zhou K, Li L et al. Transplantation of bone marrow mesenchymal stromal cells attenuates liver fibrosis in mice by regulating macrophage subtypes. Stem Cell Res Ther. 2019;10.

Publisher's note

Springer Nature remains neutral with regard to jurisdictional claims in published maps and institutional affiliations.